

Research Paper

Performance analysis of a metal hydride refrigeration system

Y.T. Ge^{*}, P.Y. Lang

Centre for Civil and Building Services Engineering (CCiBSE), UK
 School of the Built Environment and Architecture, UK
 London South Bank University, 103 Borough Road, London SE1 0AA, UK

ARTICLE INFO

Keywords:

Metal hydride refrigeration systems
 Transient model development
 Pressure
 Concentration and temperature (PCT) profiles
 Model validation and simulation
 Performance analysis and optimisation

ABSTRACT

The varying applications of metal hydride refrigeration systems, such as cold storage and space air conditioning, grant them important advantages over conventional ones. These advantages include being a low-grade heat driven, more environmentally friendly and renewable working fluid with greater compactness and fewer moving parts. However, a metal hydride refrigeration system always operates under unsteady conditions due to the cyclic hydriding and dehydriding processes involved. To analyse and optimise the metal hydride refrigeration system's design and performance, in this paper, a comprehensive transient system model has been developed with a new and revised intrinsic kinetic correlation inclusive of the essential operating controls and applicable process conditions of regeneration, cooling and transitions in between. In addition, the correlative model on the characterisation process of pressure, concentration and temperature (PCT) profiles for the metal hydride alloys employed in the system has been developed and is introduced briefly in this paper. It is integrated in the system model and ensures the accurate prediction of maximum capacities for the metal hydride isothermal desorption and absorption processes. The developed transient system model has been validated through comparison with experimental results from literature on the medium-temperature cooling process of a metal hydride refrigeration system. The model simulation is conducted for a specially designed low-temperature metal hydride refrigeration system at different operating conditions and controls. In quantity, when the high-grade heat source temperature increases from 90 °C to 120 °C, the low-grade heat source temperature increases from -20 °C to 10 °C, the medium-grade heat sink temperature decreases from 30 °C to 15 °C, and the time period for regeneration or cooling process decreases from 10 min to 4 min, the cooling COP increases by 112.0%, 136.6%, 19.3% and 31.8% respectively. The optimisation strategies for the system operating conditions and controls are therefore recommended based on the detailed performance analyses of the system simulation results.

1. Introduction

It is well-known that global warming is increasing the demand for cooling and it is now the fastest growing end-use energy demand in buildings worldwide. This high cooling demand requires a greater cooling supply and energy consumption with various refrigeration systems energised conventionally by electricity or fossil fuel combustion. The extensive fossil fuel consumption has caused serious environmental concerns such as excessive CO₂ emissions, air pollution and an energy resource crisis. It is thus essential to reduce the cooling demand and decarbonise refrigeration systems.

Hydrogen is a promising fuel to replace conventional fossil fuels in future as it is renewable and not harmful to the environment. Compared to other fuels, hydrogen has the highest energy content based on mass,

but it has a very low density at atmospheric pressure and ambient temperature and thus a very low energy content based on volume. It is therefore necessary to store hydrogen in either a vapor form with elevated pressure, or a liquid form with cryogenic technology, or a solid form with metal hydride (MH) alloys. Compared to other two hydrogen storage technologies, the hydrogen storage with MH alloys has some important advantages including an improved safety profile due to low hydrogen storage pressures, lower energy required, and greater compactness due to higher volumetric hydrogen storage capacity. The compactness of MH reactors for hydrogen desorption and absorption processes could facilitate special applications such as mechanical actuators of a pneumatic artificial muscle (PAM) [1], though advanced control strategies would be required. However, their gravimetric hydrogen storage capacities are mostly below 2% which can make an MH hydrogen storage tank far heavier than other hydrogen storage

^{*} Corresponding author at: Centre for Civil and Building Services Engineering (CCiBSE), UK.
 E-mail address: yunting.ge@lsbu.ac.uk (Y.T. Ge).

Nomenclature			
C	Hydrogen concentration (kg/kg)	U	Internal energy (J/kg)
COP	Coefficient of performance	UA	Overall heat transfer coefficient (W/K)
C_p	Specific heat at constant pressure (kJ/kg.K)	V	Volume (m ³)
D_i	Inner diameter (m)	λ	Thermal conductivity (W/m.K)
D_o	Outer diameter (m)	α	Heat transfer coefficient (W/m ² .K)
d	Diameter (m)	ϵ	Effectiveness
d_0	Reactor filter tube outer diameter (m)	<i>Subscripts</i>	
d_1	Reactor inner tube inner diameter (m)	ab	Absorption
d_2	Reactor inner tube outer diameter (m)	c	Cooling
E	Activation energy (kJ/kg)	cn	Connection pipe
fs	Slope factor	$cool$	Cooling process
ΔH	Enthalpy of metal hydride formation (J/mol)	de	Desorption
k	Coefficient	eq	Equivalent
L	Tube length (m)	f	Heat transfer fluid
m	Mass of metal hydride alloy (kg)	fi	Filter
\dot{m}	Mass flow rate (kg/s)	g	Gas
MW	Molar mass (g/mol)	h	High-grade heat source
NTU	Number of transfer units	l	Low-grade heat source
Nu	Nusselt number	m	Medium temperature heat sink
Pr	Prandtl number	max	Maximum
P	Pressure (Pa)	mid	Middle
Q	Heat transfer rate (W)	min	Minimum
\dot{Q}	Heat transfer rate (W)	MH, mh	Metal hydride
\bar{Q}	Average heat transfer rate (W)	re	Reactor
R	Universal gas constant (J/mol.K)	ref	Reference
Re	Reynolds number	reg	Regeneration process
ΔS	Entropy of metal hydride formation (J/mol.K)	t	Tube
T	Temperature (K)	$Tran-1$	Transition process from regeneration to cooling
$\Delta Time$	Time period (s)	$Tran-2$	Transition process from cooling to regeneration

technologies. To overcome this, a new structure design was applied to the MH hydrogen storage tank or heat exchanger [2]. The new design demonstrated great potential as heat exchangers with extended surface properties per volume could bear high mechanical loads, enhance heat transfer during hydrogen absorption and desorption processes, and had high hydrogen storage performance. Different reactor configurations and thermal enhancement systems applied in MH hydrogen storage technology were reviewed, compared and analysed [3]. It was found that to enhance hydrogen storage performance, the investigations of MH gravimetric hydrogen storage capacity, reaction kinetics and heat transfer management needed to be integrated.

Other than the advantages of MH hydrogen storage technology, the operating mechanism of continuous solid form hydrogen storage and discharge with MH alloys involves cyclically exothermic and endothermic heat transfer processes which can lead to different designs of energy conversion systems including refrigeration, heat pump and heat transformer etc. [4–6]. The MH refrigeration systems can have various applications such as in cold storage and space air conditioning due to their significant advantages over conventional vapor compression and absorption refrigeration systems. These include being a low-grade heat driven, environmentally friendly and renewable working fluid with greater compactness and fewer moving parts. Conversely, at the same operating conditions, the performance efficiency of an MH refrigeration system can match that of an absorption one [7]. However, for an MH refrigeration system, an MH alloy pair needs to be purposely selected based on their thermophysical properties and a specified operating condition, of which one alloy operates at high temperature or low pressure condition while the other alloy works under low temperature or high pressure state. Each MH alloy contained in a specially designed MH reactor absorbs or desorbs hydrogen and simultaneously rejects or

extracts heat to or from the outside. To ensure continuous cooling production, two pairs of MH reactors are necessarily installed in the system in which each pair is connected by a hydrogen pipe to exchange hydrogen. Moreover, uniquely, an MH refrigeration system always operates under unsteady conditions due to the cyclic MH hydrating and dehydrating processes involved. Correspondingly, dynamic state system operational investigations with both experimental and theoretical methods are essential to quantify and optimise the system performance and design [8].

A series of experimental investigations were carried out on a purposely built test rig of the MH cooling system [9,10]. In the test rig, two MH reactors with identical structure were installed and connected, in which MH alloys $\frac{5mNi}{0.95}$ and $\frac{7m}{0.09} \frac{0m}{0.05}$ were charged at different weights in the high and low temperature reactors respectively. Each MH reactor was specially designed and built with a thin MH alloy powder layer to ensure the corresponding thermal resistance was low and thus obviate the enhancement of powder thermal conductivity. Extensive experimental measurements were carried out for the test system at the operating conditions of fixed high-grade heat source temperature but varying cooling and ambient temperatures. The dynamic variations of cooling power, hydrogen exchange and hydrogen pressure development with the cooling water and ambient temperatures were measured and analysed. From the experimental investigations, the optimum cycle time of the system and the operating parameters affecting the cooling power were obtained. However, the effects of high-grade heat source temperature and transitions between regeneration and cooling processes on the system performance have not yet been tested and analysed and need to be further investigated.

The performance of an MH refrigeration system can be evaluated by the system cooling COP and specific cooling power, which are affected

by several important factors such as appropriate MH alloy selections, MH reactor design parameters, system operating conditions and controls. For an MH refrigeration system, the compositions of applicable MH alloys were optimised to maximize the hydrogen transfer capacities based on both experimental and theoretical analyses [11]. It was also found that the composition modification of each MH alloy could affect the corresponding equilibrium hydrogen pressure when the operating temperature was fixed. Moreover, the different compositions of an MH alloy could also affect other important MH properties such as hysteresis factor etc. The MH reactor designs in an MH refrigeration system normally consist of cylindrical shapes with different filter installations and heat transfer fluid tubes with MH alloy powder in between. The hydrogen accesses the MH bulk through either an inner filter tube [12,13] or a surrounding filter tube [14,15]. Regardless of the MH reactor design, it is essential to reduce the thermal resistance or distance of the MH alloy between the filter and heat transfer fluid tubes. Alternatively, the enhancement of thermal conductivity for the MH alloy was necessary by mixing it with metal foam or fibre etc [16,17]. Based on experimental investigation of MH refrigeration system, it was found that a shorter system cycle time could provide a larger cooling capacity but lower cooling COP due to a reduction in the total amount of hydrogen [18]. There is therefore an optimal cycle time where the COP could be maximised. Although experimental investigations are essential to verify concept and theoretical prediction of MH refrigeration systems, they are limited by the costs of test facilities, time consuming and large range of operating conditions. To optimise the system designs and operations, detailed and accurate system models are necessarily developed and simulated.

The modelling developments of MH refrigeration or heat pump systems are conventionally based on lumped methods and take into consideration the calculations of dynamic intrinsic kinetics of MH absorption and desorption processes, equilibrium pressures, plateau slopes, hysteresis factors, heat and mass transfers and hydrogen states etc [19–23]. Alternatively, a grey box model has been developed to predict the performance of an on-board MH hydrogen storage system [24]. Since the type of MH alloy filled in the storage tank was unknown, the system operating parameters had to be correlated with experimental measurement data by a fuel cell electric vehicle. The model could be used to predict the hydrogen capacity and evaluate the degradation degree of the storage tank.

An integrated numerical model of two MH reactors and their connection pipe was developed to predict the heat and mass transfer exchanges [19]. The one-pair MH reactor model was then extended to the two-pair MH reactor model to simulate a system such as MH heat pump or refrigeration [20]. The transient parameters simulated included reactor heat transfer, hydrogen concentration, MH pressure, and temperatures of MH and heat transfer fluid. However, the end hydrogen concentrations of both MH absorption and desorption processes were assumed as constant which are not accurate in practice. A single-stage MH heat pump model was developed and simulated at different operating conditions when various MH alloy pairs were applied [21]. By comparing the system COP and specific cooling power, an optimal MH alloy pair was suggested. Although a simple dynamic correlation of the pressure–concentration–temperature was applied and used in the model, the correlation was difficult to clarify the plateau regions at different MH operating temperatures. A single-stage MH cooling system working with one MH alloy pair was modelled [22]. The model was used to predict the effect of operating and design parameters such as heat source, sink temperatures and hydrogen charge on system performance. The research also demonstrated the importance of MH alloy choice on the system operation. Nevertheless, the limitation of hydrogen concentration during absorption or desorption process has not been included in the intrinsic kinetic equation of the dynamic model. This will affect the accuracy of the absorption and desorption process prediction. The paired reactors in the MH heat pump were studied numerically using a lumped-parameter model [23]. The model predicted

the effect of reaction rate constant on system performance in terms of MH pressures and temperature changes. However, since the pressure difference of hydrogen gas and MH equilibrium were not included in the intrinsic kinetic equation of the model, this may cause prediction uncertainty. Ultimately, some of the model assumptions require revision such as the maximum and minimum hydrogen concentrations of MH absorption and desorption processes at different temperatures and hysteresis. These parameters are always varied with operating temperatures and are critical to the accuracy of the system model. They can be calculated with a detailed and accurate model of pressure, concentration and temperature (PCT) profiles or characterisation for a particular MH alloy. In addition, a comprehensive dynamic model of the MH refrigeration system with an accurate intrinsic kinetic equation and all the essential processes including transitions needs to be further developed.

In this paper, a comprehensive MH refrigeration system model based on lumped method has been developed and explained. A new and revised intrinsic kinetic correlation for dynamic absorption and desorption processes has been proposed. In addition, the models of PCT profiles for the characterisations of MH alloy pair employed in the system have been developed and described briefly in this paper and it is thus integrated into the system model. Furthermore, four dynamic operating processes of one regeneration, one transition between regeneration and cooling, one cooling, and one transition between cooling and regeneration are calculated such that the whole system dynamic operating cycle can be modelled and simulated. The developed model has been validated with experimental results from literature. It is then applied to carry out sensitivity simulations for a low temperature MH refrigeration system at varied system operating conditions as well as controls of operating cycles. The system operations and controls can therefore be evaluated and optimised. The main contributions from this paper include a comprehensive dynamic MH refrigeration system model development and validation, a new and revised intrinsic kinetic correlation, integration of MH alloy characterisations with system model, and optimisation of the system operations and controls.

2. MH refrigeration system

The schematic diagram of an MH refrigeration system and its operating cycle to be investigated in this paper are shown in Fig. 1. As depicted, the refrigeration system consists of two identical MH alloy pairs, MH1-a&MH2-a and MH1-b&MH2-b and each pair is connected with a hydrogen flow pipe to facilitate the hydrogen exchange between two reactors. To specify, for each MH alloy pair, one operates at relatively high temperature and low pressure, namely high-temperature (HT) MH alloy, and the other works at comparatively low temperature and high pressure, specifically low-temperature (LT) MH alloy. The system operates simultaneously with these two MH alloy pairs and each pair works consecutively four processes including regeneration $a \rightarrow b$, transition from regeneration to cooling $a \rightarrow d$ and $b \rightarrow c$ (Tran-1), cooling $c \rightarrow d$, and transition from cooling to regeneration $d \rightarrow a$ and $c \rightarrow b$ (Tran-2). However, for the first half cycle, the regeneration process starts from point 'a' of HT reactor MH1-a by receiving high temperature (T_h) heat Q_{h-1} . The hydrogen is then desorbed and flows through the hydrogen pipeline and is absorbed by reactor MH2-a at point 'b' with heat release Q_{m2-1} at temperature T_m . Meanwhile, on the low pressure side, the cooling process starts from point 'c' of LT reactor MH2-b by extracting low temperature (T_l) heat Q_{l-1} from refrigerated space to produce refrigeration effect. The hydrogen is then released and passes through the hydrogen pipeline and is absorbed by reactor MH1-b at point 'd' with heat release Q_{m1-1} at temperature T_m . Once these two processes are completed, both hydrogen pipeline valves are closed immediately and two transition processes will start. For the transition process from regeneration to cooling (Tran-1), the reactor MH1-a is connected to medium temperature (T_m) heat sink and releases heat Q_{m1-2} (dot arrow line, $a \rightarrow d$). Meanwhile, the reactor MH2-a is reconnected to low temperature (T_l) heat flow Q_{l-2} ($b \rightarrow c$, dot arrow line) and cooled

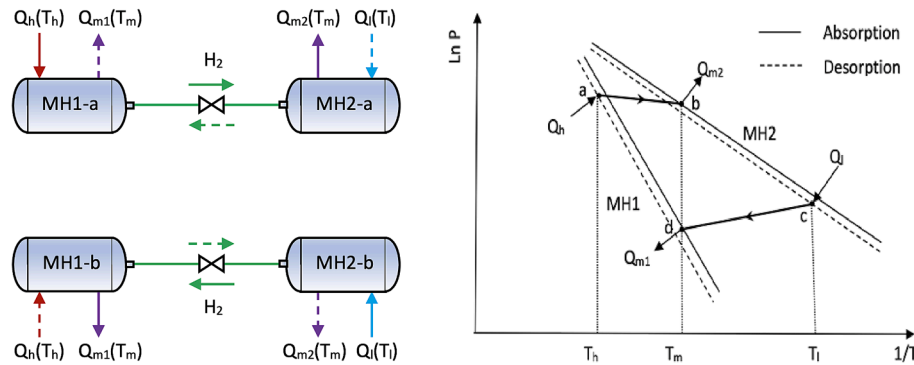


Fig. 1. Schematic diagram of a single stage metal hydride refrigeration system and its operating cycle on a Van't Hoff plot. (Q_h = heat input at high temperature heat source T_h ; Q_{m1}, Q_{m2} = heat outputs at output temperature T_m ; Q_l = Heat absorption at low temperature heat source T_l).

down from temperature T_m to T_l . For the transition process from cooling to regeneration (Tran-2), the reactor MH1-b is connected to high temperature (T_h) heat source and absorbs heat Q_{h-2} (dot arrow line, d \rightarrow a). Meanwhile, the reactor MH2-b is reconnected to medium temperature (T_m) heat flow Q_{m2-2} (c \rightarrow b, dot arrow line) and heated up from temperature T_l to T_m . Once the 1st half cycle completes, the two hydrogen pipe valves will immediately open, and the 2nd half cycle starts. For the 2nd half cycle, the pair MH1-a and MH2-a will operate through cooling and Tran-2 processes sequentially. Meanwhile, the pair MH1-b and MH2-b will run through regeneration and Tran-1 processes sequentially. The heat transfer rate and operating temperature for each process are the same as those in the 1st half cycle. The time periods for the simultaneous regeneration and cooling processes, and two transition processes for each half cycle can be set and controlled and ultimately optimised. Since the operating processes for each half cycle are the same although at different sequences, the whole system performance can be represented and analysed by one half cycle with two MH pairs operating simultaneously.

There are many MH alloy pairs which have been investigated by different researchers for the potential MH refrigeration systems. Some of these MH alloy pairs are selected and listed in Table 1 in which the application temperature ranges of T_h, T_m and T_l are listed. This can be instructive for further development in this area.

3. Characterisations of MH alloys

In this paper, the HT MH alloy $\frac{5mNi}{0.95}$ and LT MH $\frac{0.99Ti}{0.99}$ are selected for the MH refrigeration system to be investigated. The selections are based on that the measurement data from literature are applicable [9,10] for the model development and validation and they are also verified by the approach proposed by the authors for the MH alloy selections in different applications [36]. However, to facilitate efficiently a particular application, an MH alloy must firstly be characterised with a purposely built test facility to measure extensively the profiles of pressure, MH hydrogen concentration and temperature (PCT). This could be a massive and tedious task to obtain detailed PCT profiles or curves as each isotherm requires hundreds measurement points. It is thus desirable to

develop an accurate correlative model for the PCT profiles with limited measurements of thermophysical property data for the purpose of characterisation of each MH alloy. Such a correlative model or characterisation process has been developed by the authors and is described briefly in this paper. The correlative PCT MH alloy profiles can cover all applicable hydrogen storage phase regions of $\alpha, \alpha + \beta$ and β as well as the phase transition dome curve and critical point such that a PCT phase diagram for a particular MH alloy can be depicted and characterised [37]. For the MH refrigeration system, if the medium temperature T_m is maintained at 35 °C and no pressure difference for both regeneration and cooling processes is assumed, the cycle points 'a', 'b', 'c' and 'd' can be clearly demonstrated in a pressure-temperature (P-T) diagram shown in Fig. 2. As depicted, the regeneration process pressure is at 46.81 bar, cooling process pressure is at 6.28 bar, the high temperature heat source temperature T_h is at 110.12 °C while the low temperature heat source temperature T_l is at -5.17 °C. Therefore, the selected combination of HT and LT MH alloys is more suitable for the application of medium temperature refrigeration with the heat source temperature around 110 °C.

4. Modelling development of MH refrigeration system

Although the hysteresis effect can be clearly seen in the P-T diagram of Fig. 2 for each selected MH alloy, there are some assumptions in the refrigeration cycle, for example, constant pressure at either regeneration or cooling process. However, in an actual system operation, the MH pressures at points 'a' and 'c' should be higher than those at points 'b' and 'd' respectively. In addition, importantly, the MH refrigeration system always works at dynamic conditions such that the operating parameters such as temperature and pressure at each cycle point always vary with time. Therefore, to accurately predict and evaluate the system operation, dynamic system model is necessarily developed.

As explained previously, the MH refrigeration system consists of two identical MH reactor pairs and each includes a HT MH reactor and a LT MH reactor. In this paper, the structural design of cylindrical tubes is applied for each reactor, as shown in Fig. 3 for the system layout. For each MH reactor, it consists of an inlet port and an outlet port of heat transfer fluid, an outer tube, an inner tube, metal hydride alloy powder

Table 1
Potential MH alloy pairs for refrigeration systems.

MH alloy pair	T_h (°C)	T_m (°C)	T_l (°C)	Ref.
MmNi _{4.6} Al _{0.4} /MmNi _{4.6} Fe _{0.4}	80 ~ 110	25 ~ 35	5 ~ 15	[25,26]
LaNi _{4.61} Mn _{0.26} Al _{0.13} /La _{0.6} V _{0.4} Ni _{4.8} Mn _{0.2}	140 ~ 170	25 ~ 35	10 ~ 20	[15,27]
LmNi _{4.91} Sn _{0.15} /Ti _{0.99} Zr _{0.01} V _{0.43} Fe _{0.09} Cr _{0.05} Mn _{1.5}	130 ~ 160	25 ~ 35	10 ~ 20	[9]
LaNi _{4.6} Al _{0.4} /MmNi _{4.15} Fe _{0.85}	110 ~ 140	25 ~ 35	-30 ~ 15	[28,29]
Zr _{0.9} Ti _{0.1} Cr _{0.9} Fe _{1.1} /Zr _{0.9} Ti _{0.1} Cr _{0.6} Fe _{1.4}	110 ~ 140	25 ~ 35	5 ~ 15	[30,31]
LaNi _{4.6} Mn _{0.32} Al _{0.3} /La _{0.6} V _{0.4} Ni _{4.8} Mn _{0.2}	130 ~ 150	20 ~ 30	-20 ~ 5	[32]
LaNi _{4.7} Al _{0.3} /MmNi _{4.15} Fe _{0.85}	120 ~ 130	29 ~ 50	0 ~ 20	[33,34]
LmNi _{4.91} Sn _{0.15} /LmNi _{4.91} Sn _{0.15}	Compressor driven	25 ~ 35	10 ~ 20	[35]

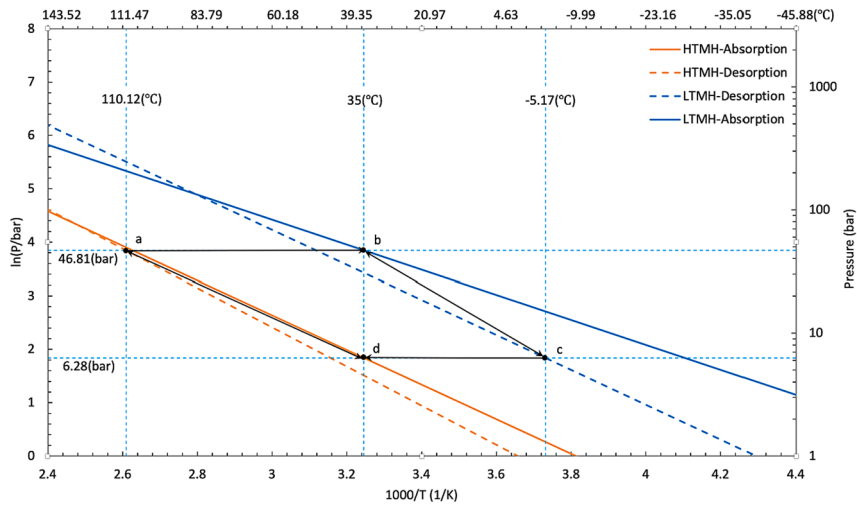


Fig. 2. A medium temperature MH refrigeration cycle shown in P-T diagram.

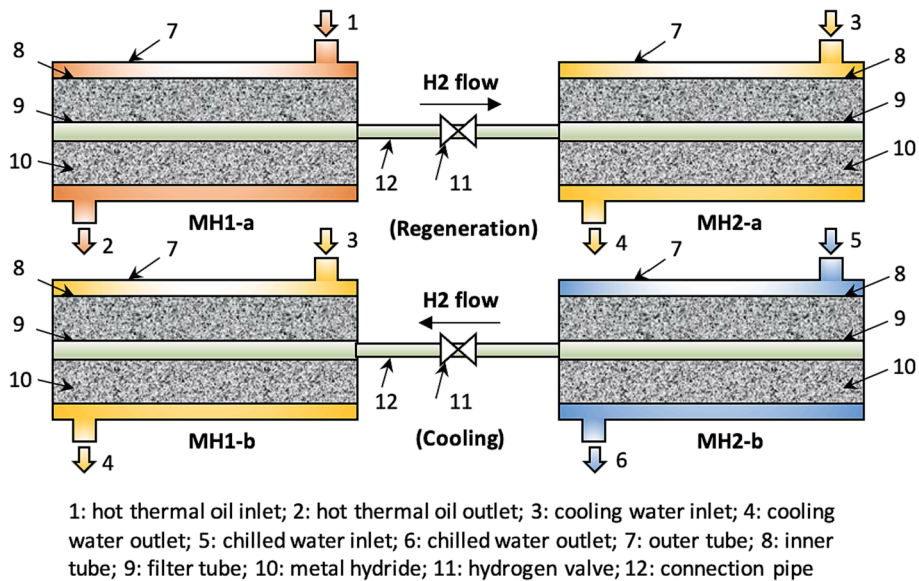


Fig. 3. Structure designs and connections of MH reactors in a MH refrigeration system.

and a filter tube. The heat transfer fluid of either hot thermal oil, cooling water or chilled water flows sequentially through inlet port, the slot between outer and inner tubes and outlet port to exchange heat with the MH reaction. The hydrogen is then absorbed into or desorbed from the MH and flows between two MH reactors along the first filter tube, connection pipe and the second filter tube. As explained in section 2, although the system operates in a number of processes, they basically can be modelled by mass and heat transfers in each reactor and mass balance in the control volume of the first filter tube, connection pipe and the second filter tube, which are described as below.

To justify, the following assumptions are made for the development of dynamic system model:

- Hydrogen behaves as an ideal gas.
- The MH lattice can be modelled with a quasi-uniform temperature model.
- The diffusivity of hydrogen through the filter tube and the MH powder does not limit the reaction.
- Due to the low gas velocity and moderate temperature, the heat transfer by convection and radiation within the MH powder bulk can be neglected.

- The MH absorption and desorption processes operate within the plateau ($\alpha + \beta$) region.

4.1. Mass transfer

When HT or LT heat is added to an MH reactor, both the temperature and pressure of the MH will increase such that hydrogen gas will be desorbed out of the MH. On the other hand, when an MH reactor absorbs hydrogen gas from the desorbed MH reactor, the reaction heat needs to be released to maintain an operational MH temperature and pressure. The hydrogen absorption or desorption or mass transfer is a dynamic process and is dependent on the MH temperature, pressure difference between the MH and its surrounding hydrogen gas, and concentration difference between instant concentration and the concentration at the process end, which can be calculated as the revised intrinsic kinetic equation (1) for both desorption and absorption processes.

$$\frac{dC}{dt} = ke^{-\frac{E}{RT}} \frac{P_g - P_{eq}}{P_{eq,max} - P_{eq,min}} |C - C_{pe}| \quad (1)$$

where, C_{pe} is the maximum plateau region ($\alpha + \beta$) concentration of absorption process or minimum plateau region ($\alpha + \beta$) concentration of desorption process.

The equilibrium pressure in the plateau region can be calculated as the modified Van't Hoff equation:

$$\ln P_{eq} = -\frac{\Delta H}{RT} + \frac{\Delta S}{R} + f_s(C - C_{mid}) \quad (2)$$

4.2. Heat transfer

For each MH reactor, the net heat transfer to the MH can cause the MH temperature to change with time, as described below:

$$mC_p \frac{dT}{dt} = \frac{m}{MW_{H_2}} \frac{dC}{dt} \Delta H + \dot{Q}_f \quad (3)$$

An effective-NTU method is applied for the calculation of heat transfer between the MH and external heat transfer fluid.

$$\dot{Q}_f = \varepsilon \dot{m}_f C_{pf} (T_f - T) \quad (4)$$

$$\varepsilon = 1 - e^{-NTU} \quad (5)$$

$$NTU = \frac{UA}{\dot{m}_f C_{pf}} \quad (6)$$

$$\frac{1}{UA} = \frac{1}{\pi d_2 L \alpha_f} + \frac{\ln \frac{d_2}{d_1}}{2\pi \lambda_i L} + \frac{\ln \frac{d_1}{d_0}}{2\pi \lambda_{MH} L} \quad (7)$$

Supposing the heat transfer fluid is under turbulent flow, the fluid heat transfer coefficient can then be calculated as:

$$Nu_f = 0.023 Re_f^{0.8} Pr_f^{0.33} \quad (8)$$

$$\alpha_f = \frac{\lambda_f Nu_f}{d_{eq}} \quad (9)$$

4.3. Mass and energy balances for hydrogen gas

For the MH refrigeration system, once the regeneration or cooling process starts to operate, the hydrogen valve connected to each process is controlled to switch on in order for the hydrogen gas within the two filter tubes and hydrogen connection pipe to reach the same pressure immediately. If the total volume of two inner filter tubes and inner hydrogen connection pipe between two connected MH reactors is set as a control volume, the corresponding mass and energy balances for each process can be calculated in Equations (10) and (11) respectively.

$$\frac{dm_g}{dt} = -m_{de} \frac{dC_{de}}{dt} - m_{ab} \frac{dC_{ab}}{dt} \quad (10)$$

$$-m_{de} \frac{dC_{de}}{dt} H_{de} - m_{ab} \frac{dC_{ab}}{dt} H_g = \frac{dm_g}{dt} U_g + m_g \frac{dU_g}{dt} \quad (11)$$

Since the hydrogen gas is assumed as an ideal gas, the following two equations are followed:

$$P_g V_g = \frac{m_g}{MW_{H_2}} RT_g \quad (12)$$

$$\frac{dP_g}{dt} = P_g \left[\frac{1}{T_g} \frac{dT_g}{dt} + \frac{1}{m_g} \frac{dm_g}{dt} \right] \quad (13)$$

4.4. Equations for transition processes

Once the regeneration and cooling processes are completed, the two hydrogen valves on those two hydrogen connection pipes are controlled to close immediately and the transition processes start between MH1-a and MH1-b, and between MH2-a and MH2-b simultaneously. For the

models of the transition processes, equations (1)–(9) can still be applied. However, the concentration variation $\frac{dC}{dt}$ will always be zero during the transition period.

4.5. System operation controls

The process of either regeneration or cooling can be controlled by a timer to fix the process operation time, and this is a simple way to control it. The process can also be controlled to complete when the minimum hydrogen flow rate is reached but an accurate hydrogen mass flow meter needs to be installed for each process. For the transition process, it can be easily controlled by a timer. Therefore, a simple way to control each operation process is by means of a timer control with a specific time period for each process which can be optimised by the model simulation or refined by the experiment.

5. Model validation

The developed MH refrigeration model has been validated with the experimental results from literature [9,10]. The test system consists of two MH reactors connected with a hydrogen pipe in which one was charged with a high temperature MH alloy $\frac{5mNi}{0.95}$ and another was charged with a low temperature alloy $\frac{6Fe}{0.99} \frac{5mNi}{0.05}$. The dynamic cooling process was measured with specific initial and operating conditions. For the initial condition, the high temperature MH equilibrium pressure, temperature and concentration were set as 4 bar, 33 °C and 0.4 wt% respectively, while the low temperature MH equilibrium pressure, temperature and concentration were fixed as 26 bar, 14 °C and 1.2 wt% individually. Water fluid was applied as the heat transfer fluid for both MH reactors. For the operating condition, the water flow rate to each reactor was set at 4 l/min while the water flow inlet temperature was the same as the initial temperature of each reactor.

The comparison between simulation and experimental results for dynamic variations of hydrogen concentrations in high and low temperature reactors during the system cooling process is shown in Fig. 4. As depicted, during the cooling process, the high temperature (HT) and low temperature (LT) MH reactors operate simultaneous hydrogen absorption and desorption processes. Although the variations of hydrogen concentration in these two processes work in opposite directions, they both change in exponential trends from start to 120 s from operation initiation. After this, there are almost no changes to the hydrogen concentrations. This implies that the time required for the cooling process can be greatly reduced. The comparison results show good alignment between simulation and experiment. In addition, the dynamic variation of hydrogen mass flow rate during the cooling process has been simulated and compared with the corresponding measurement, as shown in Fig. 5. As illustrated, there is a large increase in the hydrogen mass flow rate at the beginning of the cooling process and then an abrupt drop at the 10 s operation time. This is due to the largest initial pressure difference between these two MH reactors and the largest pressure difference reduction during the first 10 s operation. From there, the hydrogen mass flow rate decreases gradually and approaches zero when the operation time reaches 200 s. Again, the simulation results match well with the corresponding measurement data. Furthermore, the instant cooling capacity is calculated or measured based on the heat transfer fluid mass flow rate and temperature difference between fluid inlet and outlet for the LT MH reactor. The dynamic simulation and experimental results for the cooling capacity are compared and shown in Fig. 6. As demonstrated, there is a big surge in cooling capacity at the beginning of cooling process and thereafter a gradual drop in cooling capacity. It should be noted that the variation of cooling capacity does not exactly follow the change in hydrogen mass flow rate, particularly at the beginning of cooling process. This is due to a heat transfer delay in cooling capacity compared to the reaction heat from the rate of hydrogen desorption. Once more, the simulation results match well with

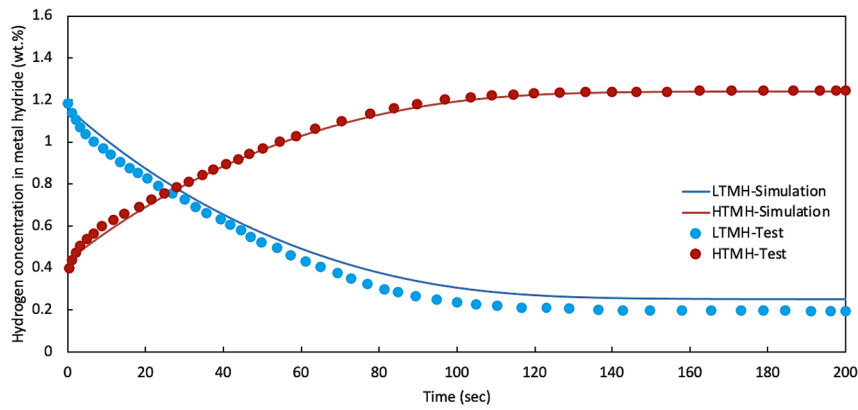


Fig. 4. Comparison between simulation and experimental results for dynamic variations of hydrogen concentrations in high and low temperature reactors during system cooling process.

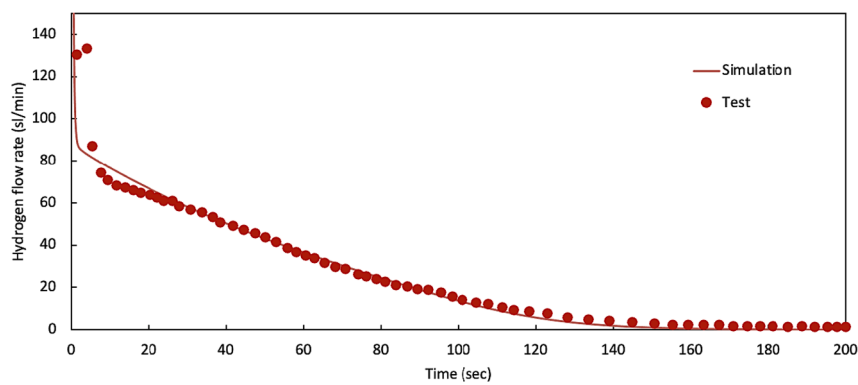


Fig. 5. Comparison between simulation and experimental results for dynamic variation of hydrogen flow rate during system cooling process.

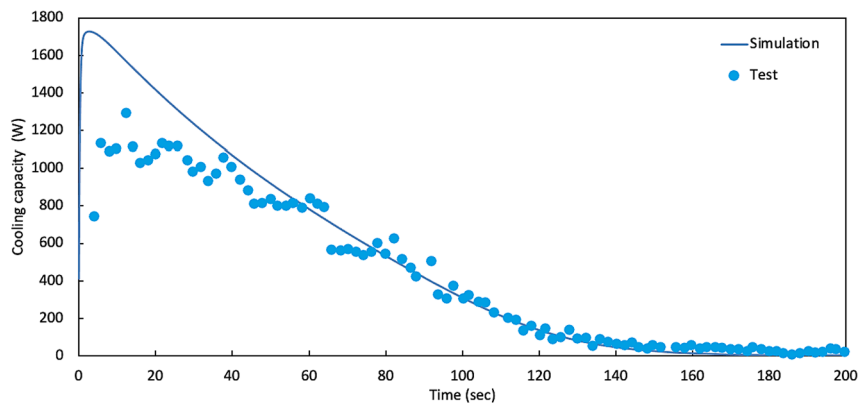


Fig. 6. Comparison between simulation and experimental results for dynamic variation of cooling capacity during system cooling process.

the corresponding measurements except for at the beginning of cooling process. Consequently, the developed dynamic MH refrigeration system model has been fairly validated.

6. Sensitive analysis and optimisation of system operation

6.1. Performance evaluation at a base operating condition

As shown in Fig. 3 for the system layout, the system operation can be represented by one pair of MH reactors connected to a hydrogen connection pipe such as MH1-a and MH2-a or MH1-b and MH2-b. However, the cooling processes for these two MH pairs should operate at different time slots in order to produce continuous cooling. Therefore,

as an example, the pair of MH1-a and MH2-a and their connection pipe operates sequentially with the processes of regeneration, transition from regeneration to cooling (Tran-1), cooling and transition from cooling to regeneration (Tran-2), and each process is controlled at different time periods. For the simulation purpose, the structural design data for each MH reactor and connection pipe are specified in Table 2. In addition, the lengths of MH reactor 1 (MH1), MH reactor 2 (MH2) and connection pipe are 1.0 m, 0.5 m and 1.0 m respectively. The MH alloy charges in MH1 and MH2 are 2 kg and 1 kg each. For the heat transfer fluids (HTFs), thermal oil and brine are used for MH1 and MH2 separately. The HTF mass flow rates for MH1 and MH2 are both fixed at 0.1 kg/s while the HTF temperature for each reactor is varied. For the initial conditions, each MH is in thermal equilibrium with that of an external HTF such that

Table 2

Design data for each MH reactor and connection pipe.

Reactor	Do_{fi} (mm)	Di_{fi} (mm)	Do_{mh} (mm)	Di_{mh} (mm)	Do_{re} (mm)	Di_{re} (mm)	Do_{cn} (mm)	Di_{cn} (mm)
MH1	12.7	9.52	33.4	27.86	42.16	36.62	12.7	9.52
MH2	12.7	9.52	33.4	27.86	42.16	36.62	12.7	9.52

the initial temperature of each MH is the same as that of external HTF. The initial MH1 concentration is the maximum concentration of the reactor at that temperature while the initial MH2 concentration is the minimum concentration of the reactor at corresponding temperature. For the base condition, the HTF temperatures for T_h , T_m and T_l are fixed at 383.15 K, 298.15 K and 283.15 K respectively. The time periods for the processes of Regeneration, Tran-1, Cooling and Tran-2 are set to 10 min, 5 min, 10 min and 5 min respectively.

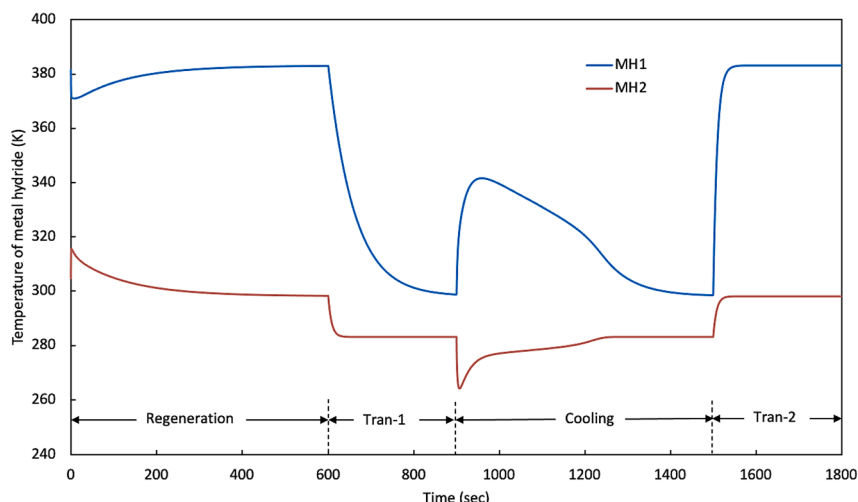
The system dynamic operation at such operating conditions is therefore simulated and demonstrated from Figs. 7 to 11 for the variations of MH temperatures, hydrogen concentrations, hydrogen and MH equilibrium pressures, hydrogen flow rate and heat transfer rates respectively. For the regeneration process, the reactors MH1 and MH2 operate respectively in hydrogen desorption with high-temperature heat addition and hydrogen absorption with medium-temperature heat release. However, in the first 15 s, those simulated operating parameters all have an abrupt reduction in terms of MH1 temperature, hydrogen concentration in MH1, MH1 equilibrium pressure and hydrogen exchange rate, or increase containing MH2 temperature, hydrogen concentration in MH2, MH2 equilibrium pressure and heat transfer rates in both reactors. After that, all these parameters increase or decrease and gradually approach respective steady-state values. To clarify, at the end of regeneration process, the MH1 and MH2 temperatures reach their corresponding HTF inlet temperatures. The hydrogen concentrations in MH1 and MH2 reach respectively their minimum and maximum values based on their corresponding temperatures. The pressures inside MH1 and MH2 come to the same value such that the hydrogen exchange rate falls to zero. Subsequently, the heat transfer rates for both reactors reduce to zero.

Once the regeneration process has completed, the Tran-1 process starts and the hydrogen valve installed in the hydrogen connection pipe is immediately closed. Meanwhile, the medium temperature heat sink and low temperature heat source are added to the reactors MH1 and MH2 respectively. Therefore, in this process, there is only heat transfer (and no hydrogen mass transfer) for each reactor. Subsequently, as shown in Fig. 7, the MH1 temperature reduces gradually due to a large temperature difference between the high temperature heat source and

the medium temperature heat sink and the larger MH alloy mass charged in MH1, while the MH2 temperature drops quickly because of the small temperature difference between the medium temperature heat sink and the low temperature heat source and also the smaller MH alloy mass charged in MH2. Both MH1 and MH2 temperatures will eventually stabilise to their corresponding HTF inlet temperatures. Since there is no hydrogen exchange in this process, the hydrogen concentration is each reactor maintains unchanged, as shown in Fig. 8 while the hydrogen mass flow rate is zero as indicated in Fig. 10. Corresponding to the temperature changes, the pressures in MH1 and MH2 vary similarly to those of temperatures, as shown in Fig. 9. However, the pressure in MH2 remains higher than that in MH1 due to different MH alloys used. It should be noted that the average pressure of MH1 and MH2 is applied to represent of the hydrogen gas pressure. Analogous to the MH temperature variations, the heat transfer rates in these two reactors vary similarly and approach zero by end of this process.

Once the Tran-1 process has completed, the cooling process will start and the hydrogen valve will open immediately while medium temperature heat sink and low temperature heat source will continue to connect to the MH1 and MH2 respectively. The MH2 and MH1 will undergo hydrogen desorption and absorption processes respectively and the desorbed hydrogen will flow from MH2 and MH1 such that the refrigeration effect will be produced in MH2. Similar to the regeneration process, the hydrogen exchange rate reaches its highest at the very beginning due to the largest pressure difference between MH2 and MH1, as shown in Fig. 10. Correspondingly, the MH temperatures, hydrogen concentrations, MH pressures, heat transfer rates all have sharp increase or decrease during the very short period. After that, these operating parameters gradually decrease or increase and eventually reach different stabilized values. These stabilized values depend on the external HTF inlet temperatures, maximum or minimum hydrogen concentrations, and time period for this process. When the process time is long enough, the hydrogen exchange rate and the heat transfer rate will all approach zero.

Once the cooling process has completed, the Tran-2 process starts and the hydrogen valve will close immediately. Meanwhile, the high temperature heat source and medium temperature heat sink will be

**Fig. 7.** Dynamic variations of MH temperatures in reactors MH1 and MH2.

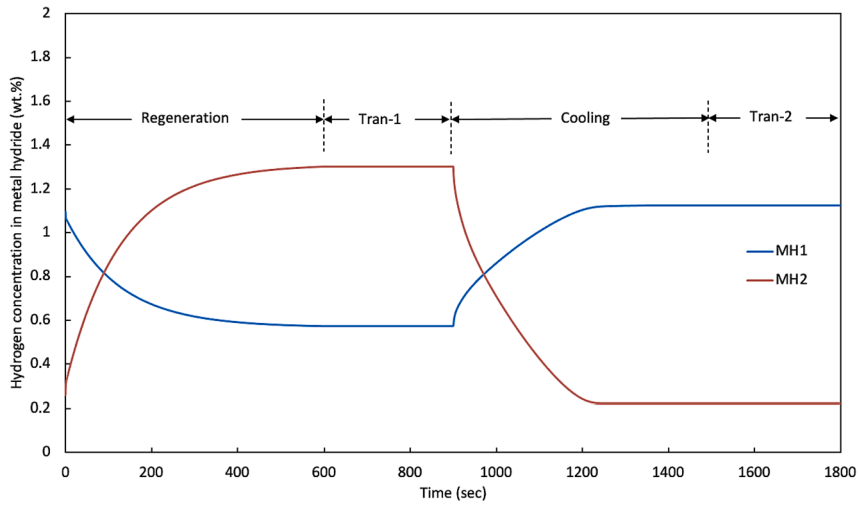


Fig. 8. Dynamic variations of MH hydrogen concentrations in reactors MH1 and MH2.

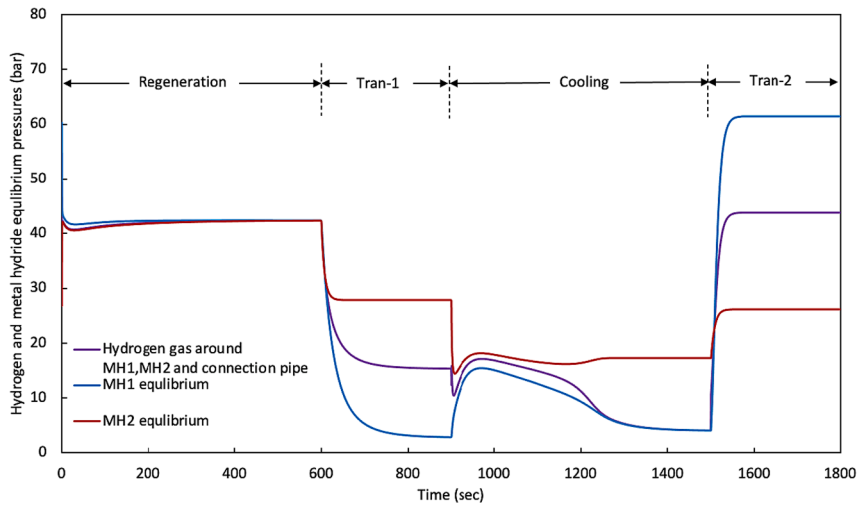


Fig. 9. Dynamic variations of MH equilibrium pressures in reactors MH1 and MH2 and external hydrogen pressure.

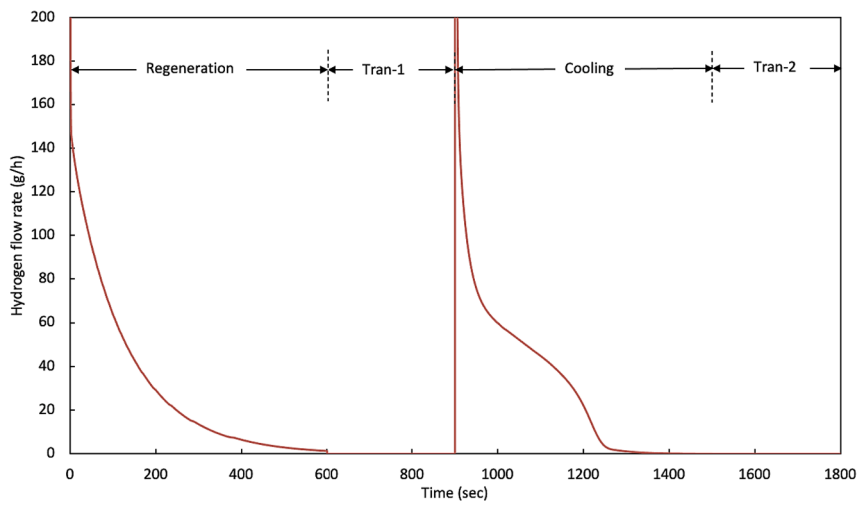


Fig. 10. Dynamic variations of hydrogen mass flow rate between reactors MH1 and MH2.

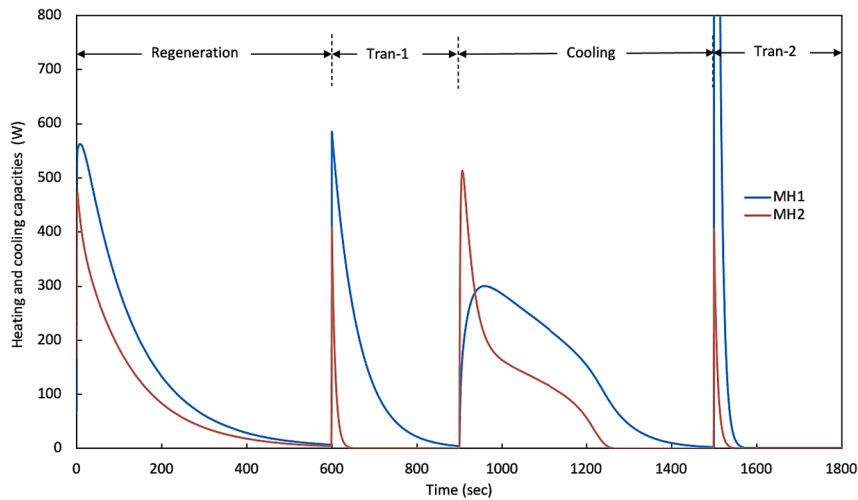


Fig. 11. Dynamic variations of heat transfer rate in reactors MH1 and MH2.

added again in the MH1 and MH2 respectively. As such, there is no mass transfer but only heat transfer during this process. Correspondingly, the hydrogen exchange rate will be zero and the hydrogen concentration in each reactor will remain unchanged. The MH temperatures, MH pressures and heat transfer rates increase or decrease abruptly at the beginning of the process and then stabilise to the values corresponding to the HTF temperatures. The heat transfer rates will fall to zero if the process time is long enough. When the process of Tran-2 completes, the cycle will repeat.

The dynamic simulation results shown in Figs. 7-11 in terms of MH temperature, hydrogen concentration, MH equilibrium pressure, hydrogen flow rate, and heating and cooling capacities have also been compared with other studies from literatures [16,17], with similar parameter variation findings. These can further verify the accuracy of the model development in this paper.

6.2. Performance comparison at different operating conditions

The system performance can be significantly affected by different operating parameters including the high-grade heat source fluid inlet temperature T_h , medium-grade heat sink fluid inlet temperature T_m , low-grade heat source fluid inlet temperature T_l , operating time period for both regeneration and cooling processes $Time_{rc}$ and operating time period for both Tran-1 and Tran-2 processes $Time_{12}$. The effective system parameters include high temperature heat input, cooling capacity and cooling COP. Since these parameters are all dynamic and varied with time, the average values during corresponding operating time periods are necessarily calculated. As explained in section 6.1, the refrigeration cycle consists of four processes including regeneration, Tran-1, cooling and Tran-2 and the average heat transfer rate of each process from starting time at '1' to end time at '2' and time period $\Delta Time$ can be calculated as:

$$\bar{Q} = \frac{\int_1^2 \dot{Q} dt}{\Delta Time} \quad (14)$$

The total high-grade heat source heat transfer rate can be calculated as:

$$\bar{Q}_h = \bar{Q}_{reg} + \bar{Q}_{Tran-2} \quad (15)$$

The net cooling capacity can be calculated as:

$$\bar{Q}_c = \bar{Q}_{cool} - \bar{Q}_{Tran-1} \quad (16)$$

The average cooling COP can therefore be calculated as:

$$COP_c = \frac{\bar{Q}_c}{\bar{Q}_h} \quad (17)$$

The effect of those operating parameters on these three performance parameters are thus simulated and demonstrated by the proposed dynamic system model. As depicted in Fig. 12, the net cooling capacity, total heat input and cooling COP all increase with a higher high-grade heat source temperature. However, the increase rate of the COP slows down with the higher heat source temperature. Quantitatively, when the high-grade heat source temperature increases from 90 °C to 120 °C, the net cooling capacity, total heat input and cooling COP increases by 347.1%, 110.9% and 112.0% respectively. As shown in Fig. 13, with the increase of the low-grade heat source temperature, the net cooling capacity increases but the total high-grade heat source heat input does not change significantly such that the cooling COP also grows although at a gradually reducing rate. For example, when the low-grade heat source temperature increases from -20 °C to 10 °C, the net cooling capacity, total heat input and cooling COP increase by 148.0%, 4.8% and 136.6% respectively. The effect of medium-grade heat sink temperature on the system performance is shown in Fig. 14. As depicted, the net cooling capacity, total heat input and cooling COP all reduce with a higher medium-grade heat sink temperature indicating that a lower medium heat sink temperature is expected. Numerically, when the medium-grade heat sink temperature increases from 15 °C to 30 °C, the net cooling capacity, total heat input and cooling COP drop by 33.4%, 17.4% and 19.3% respectively.

The time periods for regeneration and cooling processes are controlled to be the same, and this is also applied to the processes of Tran-1 and Tran-2. As shown in Fig. 15, the net cooling capacity, high-grade heat source heat input and cooling COP all decrease with longer time periods of regeneration and cooling processes, implying that shorter regeneration and cooling processes are expected. For example, when the time period for regeneration or cooling process increases from 4 min to 10 min, the net cooling capacity, total heat input and cooling COP decrease by 53.17%, 31.4% and 31.8% respectively. On the other hand, as shown in Fig. 16, the net cooling capacity and high-grade heat source heat input increases and decreases respectively with longer time period of Tran-1 and Tran-2. This is due to the smaller cooling capacity needed during the Tran-1 period while less heat input is required by the high-grade heat source heat input during Tran-2 period. Subsequently, the cooling COP increases with the longer time periods of Tran-1 and Tran-2. For instance, when the time period of Tran-1 or Tran-2 increases from 2 min to 5 min, the net cooling capacity and cooling COP increases by 25.8% and 112.1% respectively while the total heat input decreases

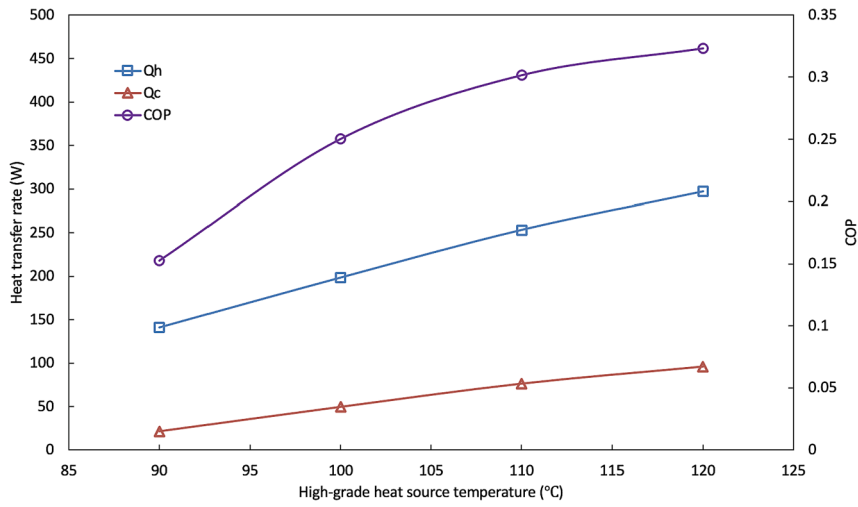


Fig. 12. The effect of high-grade heat source temperature on the system performance.

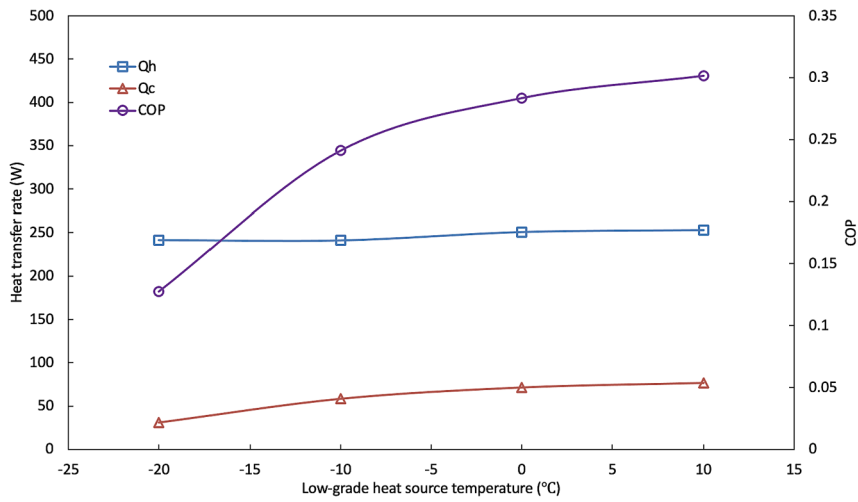


Fig. 13. The effect of low-grade heat source temperature on the system performance.

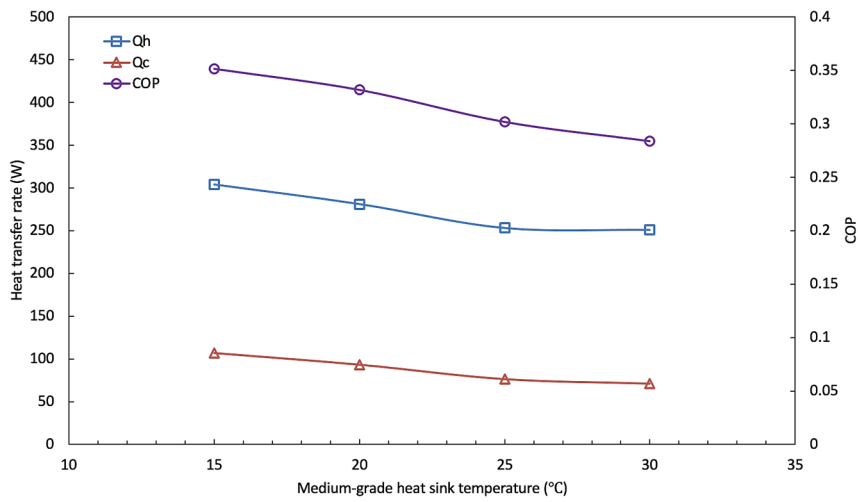


Fig. 14. The effect of medium-grade heat sink temperature on the system performance.

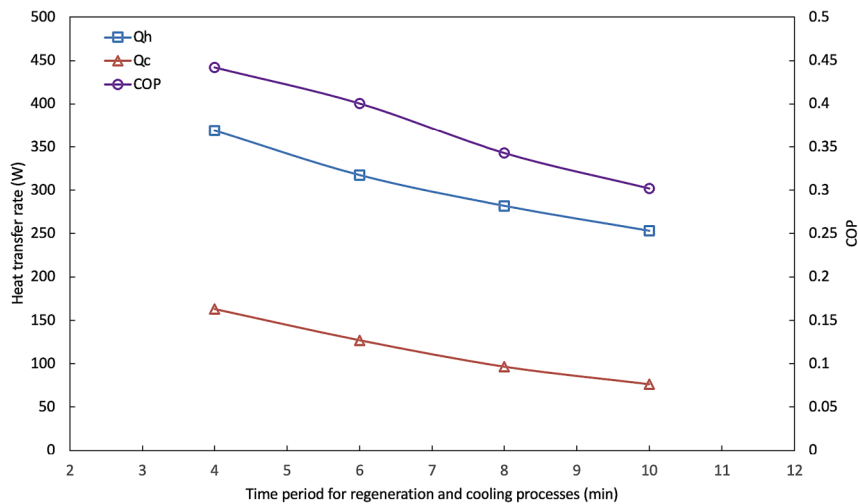


Fig. 15. The effect of time period for regeneration and cooling processes on the system performance.

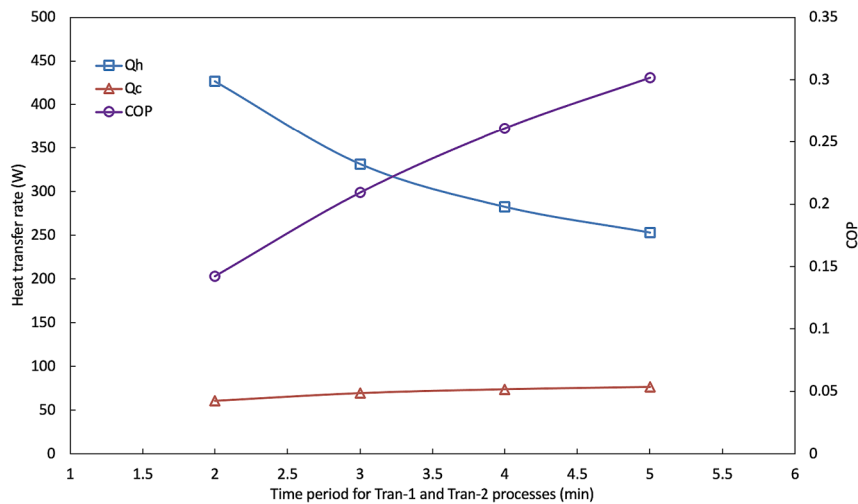


Fig. 16. The effect of time period for Tran-1 and Tran-2 processes on the system performance.

by 40.7%. The simulation results are significant to evaluate system performance at different operating conditions and optimise the system operations with a timer control for each process.

7. Conclusions

A metal hydride (MH) refrigeration system has distinct advantages over conventional refrigeration technologies in terms of being an environmentally friendly working fluid, potential for hydrogen storage, compactness and application of a low-grade heat source. However, the system always operates in dynamic processes such that all the operating and performance parameters vary with time. Correspondingly, in this paper, to analyse and optimise the performance of the MH refrigeration system, a comprehensive dynamic system model has been developed based on transient mass and heat transfer balances for each system component. To accurately predict the dynamic MH absorption and desorption processes, a new and revised intrinsic kinetic equation has been proposed and integrated into the system model. Two MH alloys have been selected for the MH refrigeration system and the MH reactor structures were designed for the modelling purpose. These two MH alloys were characterised with a purposely developed model of pressure, concentration and temperature (PCT) profiles for different MH alloys based on limited experimental results. Some important thermophysical properties and parameters for these two MH alloys can therefore be

calculated and determined including reaction enthalpy, reaction entropy, middle, minimum and maximum values of hydrogen concentration etc, which are essential for the system model development. The dynamic model has been validated with experimental results from literature and applied to system performance evaluation and comparison at different operating conditions. The simulation results found that the average system cooling capacity and COP all increase with higher high-grade and low-grade heat sources temperatures. However, with the rise in medium heat sink temperature, both average system cooling capacity and COP will reduce. In addition, with the increase of time periods for regeneration and cooling processes, the average system cooling capacity and COP will both decrease. On the other hand, with the increase of time periods for two transition processes, the average cooling capacity and COP will both increase but the high-grade heat input will decrease. The comprehensive dynamic modelling development process for the MH refrigeration system can be an efficient tool for the system performance analysis and evaluation while the simulation results from the developed model can be used for the optimisation of system design and operation.

Declaration of Competing Interest

The authors declare that they have no known competing financial interests or personal relationships that could have appeared to influence

the work reported in this paper.

Data availability

No data was used for the research described in the article.

Acknowledgements

The author would like to acknowledge the support received from Research Councils UK (RCUK, EP/T022760/1) for this research project.

References

- [1] T. Nuchkrua, T. Leephakpreeda, Actuation of pneumatic artificial muscle via hydrogen absorption/desorption of metal hydride-LaNi₅, *Adv. Mech. Eng.* 7 (2015), 364306.
- [2] L.A. Lesmana, M. Aziz, Adoption of triply periodic minimal surface structure for effective metal hydride-based hydrogen storage, *Energy* 262 (2023), 125399.
- [3] R. Sreeraj, A.K. Aadhithyan, S. Anbarasu, Integration of thermal augmentation methods in hydride beds for metal hydride based hydrogen storage systems: Review and recommendation, *J. Storage Mater.* 52 (2022), 105039.
- [4] S. Shafiee, Operational principles and effect of operating parameters on performance of metal hydride heat pumps, *Int J Refrigeration* 120 (2020) 22–30.
- [5] J.G. Park, K.J. Jang, P.S. Lee, J.Y. Lee, The operating characteristics of the compressor-driven metal hydride heat pump system, *Int. J. Hydrogen Energy* 26 (2001) 701–706.
- [6] M. Mohan, V.K. Sharma, Studies on thermodynamic performance of three stage sorption heat transformer, *Appl. Therm. Eng.* 154 (2019) 228–237.
- [7] M. Pons, F. Meunier, G. Cacciola, R.E. Critoph, M. Groll, L. Puigjaner, B. Spinner, F. Ziegler, Thermodynamic based comparison of sorption systems for cooling and heat pumping, *Int. J. Refrig* 22 (1) (1999) 5–17.
- [8] A. Demircan, M. Demiralp, Y. Kaplan, M.D. Mat, T.N. Veziroglu, Experimental and theoretical analysis of hydrogen absorption in LaNi₅-H₂ reactors, *Int. J. Hydrogen Energy* 30 (2005) 1437–1446.
- [9] J. Payá, M. Linder, E. Laurien, J.M. Corberán, Dynamic model and experimental results of a thermally driven metal hydride cooling system, *Int. J. Hydrogen Energy* 34 (7) (2009) 3173–3184.
- [10] M. Linder, R. Mertz, E. Laurien, Experimental results of a compact thermally driven cooling system based on metal hydrides, *Int. J. Hydrogen Energy* 35 (14) (2010) 7623–7632.
- [11] H. Nakamura, Y. Nakamura, S. Fujitani, I. Yonezu, A method for designing a hydrogen absorbing LaNi_{5-x-y}Mn_xAl_y alloy for a chemical refrigeration system, *J. Alloy. Compd.* 252 (1-2) (1997) 83–87.
- [12] H.-P. Klein, M. Groll, Development of a two-stage metal hydride system as topping cycle in cascading sorption systems for cold generation, *Appl Thermal Eng* 22 (6) (2002) 631–639.
- [13] A.S. Chernikov, L.A. Izhvanov, A.I. Solovey, V.P. Frolov, Y.I. Shanin, An installation for water cooling based on a metal hydride heat pump, *J. Alloy. Compd.* 330–332 (2002) 907–910.
- [14] F. Qin, J. Chen, M. Lu, Z. Chen, Y. Zhou, K.e. Yang, Development of a metal hydride refrigeration system as an exhaust gas- driven automobile air conditioner, *Renew. Energy* 32 (12) (2007) 2034–2052.
- [15] J. Ni, H. Liu, Experimental research on refrigeration characteristics of a metal hydride heat pump in auto air- conditioning, *Int. J. Hydrogen Energy* 32 (13) (2007) 2567–2572.
- [16] W. Supper, M. Groll, U. Mayer, Reaction kinetics in metal hydride reaction beds with improved heat and mass transfer, *J. Less-Common Met.* 104 (2) (1984) 279–286.
- [17] A. Isselhorst, M. Groll, Two-stage metal hydride heat transformer laboratory model, *J. Alloy. Compd.* 231 (1-2) (1995) 888–894.
- [18] T. Imoto, T. Yonesaki, S. Fujitani, I. Yonezu, N. Hiro, K. Nasakot, T. Saito, Development of an F-Class refrigeration system using hydrogen-absorption alloys, *Int. J. Hydrogen Energy* 21 (1996) 451–455.
- [19] M. Gambini, Metal hydride energy systems performance evaluation, Part A: dynamic analysis model of heat and mass transfer, *Hydrogen Energy* 19 (1994) 67–80.
- [20] M. Gambini, Metal hydride energy systems performance evaluation, Part B: performance analysis model of dual metal hydride energy systems, *Hydrogen Energy* 19 (1994) 81–97.
- [21] A. Satheesh, P. Muthukumar, Performance investigations of a single-stage metal hydride heat pump, *Int. J. Hydrogen Energy* 35 (13) (2010) 6950–6958.
- [22] J. Payá, M. Linder, R. Mertz, J.M. Corberán, Analysis and optimization of a metal hydride cooling system, *Int. J. Hydrogen Energy* 36 (1) (2011) 920–930.
- [23] H. Bjurström, S. Suda, The metal hydride heat pump: dynamics of hydrogen transfer, *Int. J. Hydrogen Energy* 14 (1) (1989) 19–28.
- [24] D. Zhu, Y. Ait-Amirat, A. N'Diaye, A. Djerdir, New dynamic modeling of a real embedded metal hydride hydrogen storage system, *Int. J. Hydrogen Energy* 44 (55) (2019) 29203–29211.
- [25] A. Satheesh, P. Muthukumar, A. Dewan, Computational study of metal hydride cooling system, *Int. J. Hydrogen Energy* 34 (7) (2009) 3164–3172.
- [26] A. Satheesh, P. Muthukumar, A. Dewan, Modelling of metal hydride based cooling system. In: *National Conference on Refrigeration and Air Conditioning (NCRAC)*, 8-10 January 2009, IIT Madras, India, 61.
- [27] F. Qin, J. Chen, M. Lu, Z. Chen, Y. Zhou, K.e. Yang, Development of a metal hydride refrigeration system as an exhaust gas- driven automobile air conditioner, *Renew. Energy* 32 (12) (2007) 2034–2052.
- [28] A.S. Chernikov, L.A. Izhvanov, A.I. Solovey, V.P. Frolov, Y.I. Shanin, An installation for water cooling based on a metal hydride based heat pump, *J. Alloy. Compd.* 330–332 (2002) 907–910.
- [29] L.A. Izhvanov, A.I. Solovey, V.P. Frolov, Y.I. Shanin, Metal hydride heat pump-new type of heat converter, *Int. J. Hydrogen Energy* 21 (1996) 1033–1038.
- [30] S.G. Lee, Y.K. Kim, J.Y. Lee, Operating characteristics of metal hydride heat pump using Zr-based laves phases, *Int. J. Hydrogen Energy* 20 (1995) 77–85.
- [31] J.M. Park, J.Y. Lee, Hydrogenation characteristics of the Zr_{1-x}Ti_xCr_{1-y}Fe_{1-y} laves phase alloys, *J. Less-Common Met.* (1990;160:259e71.).
- [32] T. Imoto, T. Yonesaki, S. Fujitani, I. Yonezu, N. Hiro, K. Nasako, Development of an F-class refrigeration system using hydrogen-absorbing alloys, *Int. J. Hydrogen Energy* 21 (1996) 451–455.
- [33] D.M. Gruen, M. Mendelsohn, I. Sheft, G. Lamich, Materials and performance characteristics of the HYCSOS chemical heat pump and energy conversion systems, In: *Hydrogen energy systems, proceedings of second world hydrogen energy conference, Zurich, vol. 4. Pergamon Press; 21–24 Aug. 1978. p. 1931–46.*
- [34] D.M. Gruen, M.H. Mendelsohn, I. Sheft, Metal hydrides as chemical heat pumps, *Sol. Energy* 21 (2) (1978) 153–156.
- [35] P. Muthukumar, M.S. PatilNithin, N. Raju, M. Imran, Parametric investigations on compressor-driven metal hydride based cooling system, *Appl. Therm. Eng.* 97 (2016) 87–99.
- [36] Y.T. Ge, P.Y. Lang, Alloy selections in high-temperature metal hydride heat pump systems for industrial waste heat recovery, *Energy Rep.* 8 (2022) 3649–3660.
- [37] Y.T. Ge, P.Y. Lang, Characterisation of pressure-concentration-temperature (PCT) profiles with limited measurement data for different metal hydride hydrogen storage alloys, Internal Research Project Report (2023).